Distributed Transverse Stress Sensor Based on Mode Coupling in Weakly-Coupled FMF

Junchi Jia ⑩, Yu Yang ⑩, Mingqing Zuo, Jian Cui, Yuyang Gao ⑩, Jinyi Yu, Huang Yu, Zhenrong Zhang ⑩, Zhangyuan Chen ⑩, Yongqi He, *Member, IEEE*, and Juhao Li ⑩

Abstract—**Distributed optical fiber sensors (DOFSs) have faced the challenge of measuring transverse stress along the fiber and the current main approach has been based on polarization coupling effect in polarization-maintaining fibers (PMFs), which has short sensing length and high dependence on direction of exerted stress. Instead, here we propose a novel distributed transverse stress sensor (DTSS) based on coupling effect between linearly-polarized (LP) modes in weakly-coupled few-mode-fibers (FMFs). In this scheme, multiple LP modes could be considered as independent spatial channels without stress perturbation because of ultralow inherent modal crosstalk, while quantifiable and spatially-resolvable mode coupling for a probe signal will occur under transverse stress satisfying phase-matching conditions. A proof-of-concept DTSS system is verified based on weakly-coupled two-mode fibers and mode-selective couplers for mode conversion. Moreover, we show that the scheme is little affected by mild common parameters including temperature, strain, twist, direction of stress, or state-of-polarization (SOP), which is crucial for accurate stress analysis under complex environmental conditions. The proposed DTSS scheme has simple structure, high flexibility for different sensing ranges and resolutions, and high collaborating capability with other sensing mechanisms.**

Index Terms—**Distributed transverse stress sensor, few-mode fibers, mode coupling effect, optical fiber sensors.**

I. INTRODUCTION

IN RECENT years, distributed optical fiber sensors (DOFSs) utilizing the entire fiber as both the sensing element and transmission medium have experienced an explosive growth [1]–[3], in which intensity, phase, or frequency changes of probe light caused by a specific parameter under investigation along the fiber can be detected with spatial resolution. Typically, a DOFS should be only sensitive to the parameter under test and robust against effect of other parameters [4]. Otherwise, the measurement uncertainty will greatly limit its practical applications. Multiple-parameter measurement may improve the tolerance, but with the cost of greatly-raised system complexity [5]. So DOFSs with simple system structure, wide range of operating conditions, and high tolerance to effect of undesired parameters are highly welcomed.

Currently, the Raman, Brillouin, and Rayleigh scattering effects in single-mode fibers (SMFs) have received frequent usage and the typical parameters have been temperature, vibration, and strain [6]. However, distributed transverse stress sensors (DTSSs) have been little studied, which could find unique applications in many fields such as geological disaster monitoring and early warning, structural health monitoring, medical monitoring, manufacturing process monitoring, and so on [7], especially in pressure monitoring area, including oil/gas downhole and pipeline, geotechnical engineering, water distribution and sewerage utilities [8], [9]. In these cases, the sensing of transverse stress is more effective and cannot be replaced by other sensing mechanisms. However, the current main approach for DTSSs is based on polarization coupling in polarization-maintaining fibers (PMFs) [10]–[12], the immunity of which to effect of undesired parameters should be greatly improved for practical applications because of high dependence on direction of exerted stress and various force perturbations degrading polarization maintenance such as twist and strain [13]. Moreover, the fiber length is always less than 1-km for the large inherent coupling between polarizations [14].

In this paper, we propose a novel DTSS mechanism based on linearly-polarized (LP) mode coupling effect under transverse stress in weakly-coupled few-mode fibers (FMFs), which is quite different with previous studies for DOFSs over FMFs such as monitoring multiple parameters simultaneously with multiple LP modes or improving system performance utilizing transmission characteristics of FMFs [15]. There also have been some studies for stress measurement utilizing mode coupling effect [16]–[19], but all of them are based on fiber gratings, which is only suitable for single or multiple-point measurements instead of distributed sensing. In the proposed scheme, multiple LP modes in the FMF could be considered as independent spatial channels because of ultralow inherent modal crosstalk, while a transverse stress may induce quantifiable

Junchi Jia, Yu Yang, Mingqing Zuo, Jian Cui, Yuyang Gao, Jinyi Yu, Zhangyuan Chen, Yongqi He, and Juhao Li are with the State Key Laboratory of Advanced Optical Communication Systems and Networks, Department of Electronics, Peking University, Beijing 100871, China (e-mail: jiajunchi@pku.edu.cn; yangyupku@pku.edu.cn; zuomq@pku.edu.cn; cjyx@pku.edu.cn; yuyanggao@pku.edu.cn; yujinyi@pku.edu.cn; chenzhy@pku.edu.cn; heyongqi@pku.edu.cn; juhao_li@pku.edu.cn).

Huang Yu is with the Fiberhome Fujikura Optics Technology Company, Ltd., Wuhan 430074, China (e-mail: yuhuang@fiberhome.com).

Zhenrong Zhang is with the Guangxi Key Laboratory of Multimedia Communications and Network Technology, Guangxi University, Nanning 530004, China (e-mail: zzr76@gxu.edu.cn).
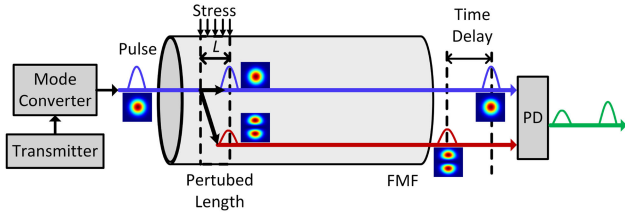
Digital Object Identifier 10.1109/JPHOT.2021.3136257

Fig. 1. Schematic structure of a two-mode DTSS.

Fig. 2. Schematic diagram of the fiber core cross-section under displacement.

and spatially-resolvable mode coupling for a probe signal under phase-matching conditions without any fiber grating structure. So this scheme has very high requirements for ultralow-modal-crosstalk FMFs and high-selectivity mode exciters. We have experimentally demonstrated 55-km weakly-coupled two-mode fiber (TMF) transmission [20], which makes the proposed scheme possible. We theoretically analyze the relationship between mode coupling and transverse stress and experimentally demonstrate a proof-of-concept DTSS system for a two-mode case. Then the immunity of the proposed DTSS to effect of common parameters are experimentally investigated. Part of results were briefly reported in a recent conference presentation [21].

II. PRINCIPLE OF OPERATION

Although different kinds of external forces may induce different coupling behaviors among multiple modes in an FMF [22], we only consider a two-mode case in this paper, the DTSS mechanism of which is shown in Fig. 1. At the transmitted side, an optical pulse signal generated by the transmitter is launched into the LP_{01} mode utilizing a mode converter. The TMF is designed to support only the LP_{01} and LP_{11} modes with large effective index difference (Δn_{eff}), so that the modal crosstalk between them is ultralow and only the LP_{01} mode signal is received at the receiver without the influence of transverse stress. When transverse stress is applied with the proper phase-matching condition at a specific position along the TMF, part of signal power in the LP_{01} mode will be coupled to the LP_{11} mode. At the receiver, a photodiode (PD) with a multi-mode fiber (MMF) pigtail can be used to detect signals in both modes. Since the two LP modes in the weakly-coupled FMF always have large differential mode group delay (DMD) coefficient κ, the signals in the two modes will arrive to the fiber end with a time delay τ, and the distance D from the event position to the fiber end can be determined by τ/κ. We can see that the scheme has very simple structure and the transmitting, receiving, and timing units may refer to those in a typical optical time-domain reflectometer (OTDR) [23]. In addition, the flexible sensing range, resolution, and sensitivity can be realized by adjusting parameters of the TMF including the core radius, index profile and index difference between the core and cladding. It should be noted that the sensitivity of the proposed DTSS may be decided by and inversely related to the Δn_{eff} between modes. As the Δn_{eff} increases, the coupling efficiency decreases, and so does the sensitivity.

We adopt a simplified fiber deformation model for a two-mode case to investigate the relation between coupled mode power
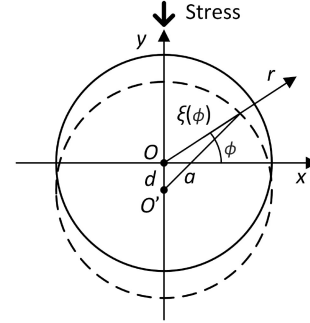
and applied transverse stress [17]. Assuming that the step-index circular-core (SI-CC) TMF removed of the coating is subjected to a small transverse stress in the y-axis, the fiber core will suffer from the slight effects including birefringence, elliptical deformation, and displacement perturbation [17], among which only displacement perturbation is important because coupling can only occur between two LP modes when their azimuthal orders differ by ± 2 for elliptical deformation and that is dissatisfied in TMFs [22], and birefringence can only cause coupling between the polarization components of one mode and we only consider the superposition of them [22].

The core cross-section under displacement in the stress direction is shown in Fig. 2. For a given $r - \phi$ circular coordinate system, the x-axis direction is $\phi = 0$, the solid (dotted) circle centered at O (O') is the core of the unperturbed (perturbed) fiber. And a is the core radius, d is the core displacement, $\xi(\phi)$ is the distance from the unperturbed core center O to the perturbed core boundary. As transverse stress is applied, a compression is created and the diameter of the fiber cladding decreases by a compression value d_m [24], so the fiber core displacement d will be $d_m/2$ [25], and $\xi(\phi)$ can be given by

$$\xi(\phi) \approx -d\sin(\phi) + a$$
$$= -\frac{V_m F}{2}\left[1 + \ln\left(\frac{L^2}{V_m F b}\right)\right]\sin(\phi) + a. \quad (1)$$

Where F is transverse stress, b is the cladding radius, L is the interaction length, and $V_m = (1 - \sigma^2)/\pi E$ (σ is Poisson's ratio and E is Young's modulus). The approximation is good as $\xi(\phi) = -d\sin(\phi) + [a^2 - d^2\cos(\phi)]^{1/2}$.

Then the coupling coefficient under displacement is analyzed, and that between the LP_{01} and LP_{11b} modes (has the mode lobe orientation parallel to the y-axis) can be given by [26]

$$K_{01,11b} = \frac{\omega}{4}\int_0^{2\pi}\int_a^{\xi(\phi)}\varepsilon_0\left(n_{co}{}^2 - n_{cl}{}^2\right)E_{01}(r,\phi)$$

$$\times E_{11b}(r,\phi)\, r dr d\phi, \quad (2)$$

where ω is the angular frequency, ε_0 is the vacuum permittivity, $n_{co}(n_{cl})$ is the core (cladding) refractive index (RI), and E_{01} and E_{11b} are the transverse field components of the LP_{01} and LP_{11b}

modes, which can be given by [27]

$$E_{01}(r, \phi) = A_0 J_0(ur/a), \qquad\qquad 0 < r \le a$$
$$E_{01}(r, \phi) = A_0 J_0(u) K_0(wr/a)/K_0(w), \quad r > a \qquad (3)$$

and

$$E_{11b}(r, \phi) = A_1 J_1(ur/a)\sin(\phi), \qquad\qquad 0 < r \le a$$
$$E_{11b}(r, \phi) = A_1 J_1(u) K_1(wr/a)\sin(\phi)/K_1(w), \quad r > a \qquad (4)$$

where A_l is the normalized amplitude of the transverse field components, J_l is the Bessel function of the first kind, K_l is the modified Bessel function of the second kind, l is the azimuthal order of the mode, u and w are the transverse propagation constants in the core and cladding. Here, $K_{01,11a}$ and $K_{11a,11b}$ are not presented because it's clear that the integral for calculating them is zero. So cross coupling will only occur between the LP_{01} and LP_{11b} modes. And since $\xi(\phi)$ is very close to a under slight perturbation, we can approximate $r = a$. Therefore, by substituting $r = a$, (1), (3) and (4) into (2), we have

$$K_{01,11b} = -\frac{\pi\omega\varepsilon_0\left(n_{co}^2 - n_{cl}^2\right)}{8} A_0 A_1 J_0(u_{01}) J_1(u_{11b}) aFV_m$$
$$\times \left[1 + \ln\left(\frac{L^2}{V_m Fb}\right)\right]. \qquad (5)$$

Let c_{01} and c_{11b} be the modal complex amplitudes of the LP_{01} and LP_{11b} modes. Based on coupled-mode theory, c_{01} and c_{11b} on z axis can be given by [28]

$$\begin{bmatrix} \frac{dc_{01}(z)}{dz} \\ \frac{dc_{11b}(z)}{dz} \end{bmatrix} = -j \begin{bmatrix} \beta_{01} + K_{01,01} & K_{01,11b} \\ K_{01,11b}{}^* & \beta_{11b} + K_{11b,11b} \end{bmatrix} \begin{bmatrix} c_{01}(z) \\ c_{11b}(z) \end{bmatrix}, \qquad (6)$$

where β_{01} and β_{11b} are the propagation constants of the LP_{01} and LP_{11b} modes without perturbation. When only the LP_{01} mode is incident, expressed as $c_{01}(0) = 1$ and $c_{11b}(0) = 0$, the power coupling ratio which is the power of the LP_{11b} mode versus the total power at $z = L$ can be given by [28]

$$H = \frac{|c_{11b}(L)|^2}{|c_{01}(0)|^2} = (2K_{01,11b}/s)^2 \sin^2(sL/2), \qquad (7)$$

where s is the propagation constant difference of the LP_{01} and LP_{11b} modes under perturbation and can be given by $s = [(\Delta\beta + K_{01,01} - K_{11b,11b})^2 + (2K_{01,11b})^2]^{1/2}$, in which $\Delta\beta = \beta_{01} - \beta_{11b}$. Because $\Delta\beta$ in weakly-coupled TMFs is always very large and $K_{01,01}$-$K_{11b,11b}$ and $K_{01,11b}$ are very small compared with $\Delta\beta$ under slight perturbation [12], there will be $s \approx \Delta\beta$. By substituting (5) and $s \approx \Delta\beta$ into (7), we have

$$H \approx \frac{C^2 F^2 \left[1 + \ln\left(L^2/V_m Fb\right)\right]^2}{\Delta\beta^2}\sin^2\left(\frac{\Delta\beta L}{2}\right). \qquad (8)$$

Where C is a constant for a given TMF, and can be given by $C = \pi\omega\varepsilon_0(n_{co}^2 - n_{cl}^2)A_0 A_1 J_0(u_{01}) J_1(u_{11b}) V_m/4$. It should be noted that although the H is only related to LP_{11b} mode but not the LP_{11a} mode, the total power of the LP_{11} mode and the H are related if we detect the LP_{11a} and LP_{11b} as a whole.

Moreover, for a specific sensing fiber and fixed wavelength λ of the launched signal, the C, V_m, b and $\Delta\beta$ will not change under slight stress perturbation with a given L. So from (8) we can see that H is only related to the magnitude of transverse stress F, which means that the proposed DTSS scheme is quantifiable. The theoretical analysis shows that the mode coupling induced by transverse stress in weakly-coupled FMFs mainly comes from the displacement perturbation of the fiber core and the mode coupling is insensitive to common parameters including temperature, strain, twist, direction of stress, or state-of-polarization (SOP) that do not contribute to the displacement perturbation, which is crucial for accurate stress analysis under complex environmental conditions.

III. EXPERIMENTAL SETUP AND RESULTS

The experimental setup to verify the proposed DTSS scheme is shown in Fig. 3(a). At the transmitter (TX), an electric pulse signal with the pulse width of 50-ps and the repetition frequency of 10-MHz is generated by the arbitrary waveform generator (AWG, Tektronix, AWG70002A). Light from a 1550-nm distributed feedback laser (DFB, Southern photonics, TLS150D) is modulated by an optical intensity modulator (IM, Fujitsu, FTM7938EZ) driven by the electric pulse signal. Then the optical pulse signal is amplified by an Erbium-doped fiber amplifier (EDFA, Amonics, AEDFA-C-PM-23) and launched into the LP_{01} mode of the TMF utilizing a mode-selective coupler (MSC) acting as a mode converter, which is fabricated by tapering the TMF with SMFs according to phase matching conditions [29]. The insertion loss of the MSC is about 0.2-dB and the modal crosstalk is about -30.3-dB. The index profile of the TMF and effective index of the LP_{01} and LP_{11} modes are shown in Fig. 3(b). The radii of the core and cladding are about 6.9 and $62.5 - \mu$m, respectively, and the relative core-cladding index difference Δ is 0.47%. So the SI-CC FMF has a normalized frequency V of 3.9 and supports only the LP_{01} and LP_{11} modes with a Δn_{eff} of 2.47×10^{-3}. There are three TMF links for single-point, multiple-point, and immunity tests, respectively. At the receiver (RX), a PD (Conquer, KGPD20GMMFA) with an MMF (YOFC, OM4) pigtail is employed to detect signals for both modes, followed by an oscilloscope (Tektronix, DPO72004C) with a maximum sample rate of 100-GSa/s to capture the waveforms. A single-axis translation stage attached with an acrylic plate is utilized to apply stress with a fixed interaction length L of 0.3-mm to the TMF, the structure of which is shown in Fig. 3(c).

The single-point stress sensing capability for the proposed DTSS scheme is first investigated utilizing the experimental setup with Link 1 in Fig. 3(a). Fig. 4(a) shows the waveforms of the received signals captured by the oscilloscope with different applied transverse stress of 0, 0.1, 0.2, and 0.3-kgf, respectively, for which the relative intensity is calculated by subtracting the corresponding peak value of the received LP_{01} pulse from the waveforms. We can see that the inherent modal crosstalk of the TMF is well suppressed and only two peaks are observed corresponding to the launched LP_{01} signal and stress-induced LP_{11} signal. The time interval between them is 11.86-ns. Since
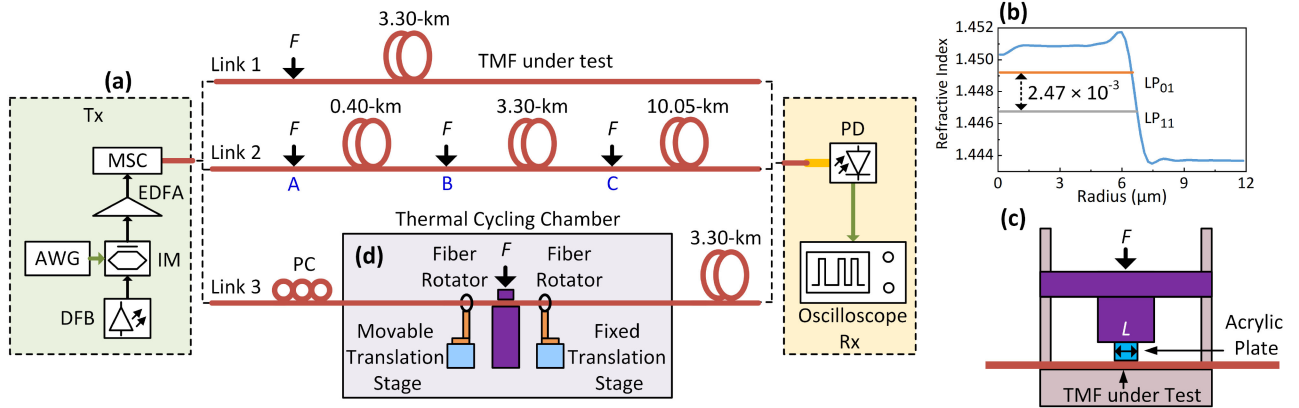
Fig. 3. (a) Experimental setup for the proposed DTSS scheme. (b) The index profile of the TMF and effective index of the LP_{01} and LP_{11} modes. (c) Apparatus to apply transverse stress. (d) Experiment setup for measuring the influence of temperature, strain, twist, stress direction, and state-of-polarization changes of incident light. Tx: Transmitter. DFB: Distributed feedback laser. IM: Intensity modulator. AWG: Arbitrary waveform generator. EDFA: Erbium-doped fiber amplifier. MSC: Mode-selective coupler. TMF: Two-LP-mode fiber. F: Transverse stress. L: Interaction length. PC: Polarization controller. Rx: Receiver. PD: Photodetector.
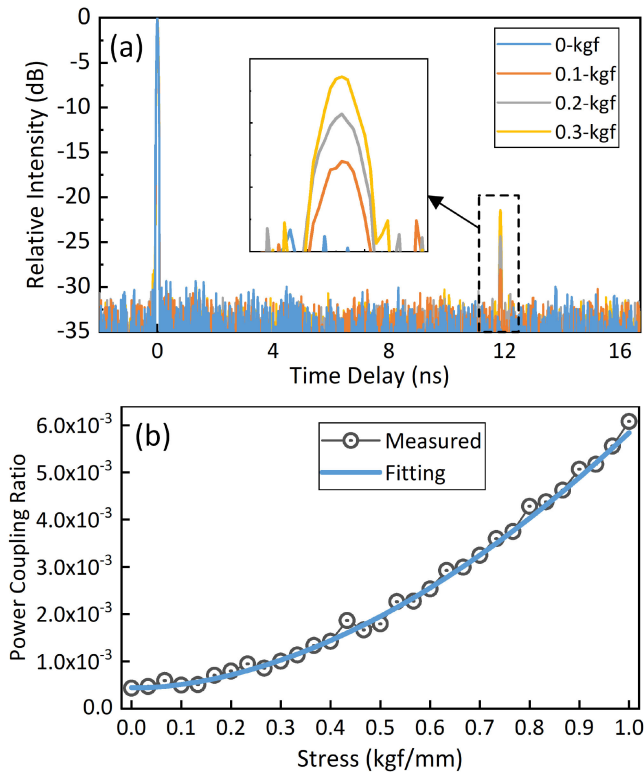

Fig. 4. (a) Relative intensity of the received signal. (b) Measured power coupling ratio as a function of transverse stress. The fitting and measured data are denoted as black dots and blue line.
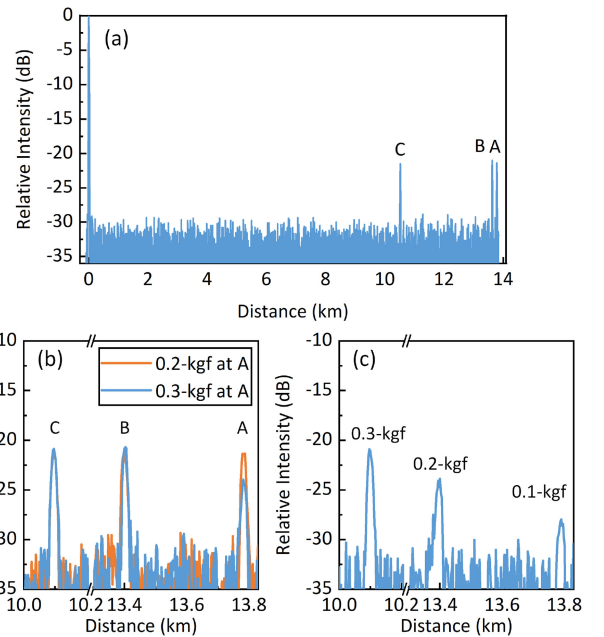

Fig. 5. (a) Relative intensity of the received signal for multi-point measurement. (b) Influence measurement between mode coupling of multiple points. (c) Feasibility measurement of applying different stresses at different points.

the DMD coefficient is 3.76-ps/m, the calculated position for the applied stress is 3.15-km from the fiber end at the receiver, which agrees with the fiber length. The DMD coefficient is obtained by dividing the time delay between the LP_{01} and LP_{11} signals propagating through the fiber in Link 1 by the fiber length, for which the time delay can be measured by the waveforms captured by the oscilloscope, while the fiber length can be measured with OTDR (EXFO FTB-1). The inset graph depicts the enlarged waveforms for LP_{11} pulses and we can see that the

power of the stress induced LP_{11} peak increases with the applied transverse stress. The power coupling ratio between the received LP_{01} and LP_{11} pulses versus the applied transverse stress is depicted in Fig. 4(b). Considering the attenuation difference for the two modes and bias due to noise, the curve of power coupling ratio can be fitted according to (8) utilizing the Least-square Method.

Then multiple-point sensing capability for the proposed DTSS is investigated utilizing the experimental setup with Link 2 in Fig. 3(a). The Link 2 consists of three fiber spools with lengths of about 0.40, 3.30, and 10.05-km, respectively. 0.3-kgf stress is simultaneously applied at points A, B, and C near each connection between fiber spools and Fig. 5(a) shows the relative

intensity of the received signal as a function of distance from the output end of the fiber. The distance is converted from the time delay using the DMD coefficient. We can see that 3 peaks exist corresponding to points A, B, and C with the measured positions of 13.790, 13.399, and 10.096-km, which are in good agreement with the configurations. And the spatial resolution is measured as about 17-m according to the full width at half maxima (FWHM) of the LP_{11} pulse. Moreover, the spatial resolution can be greatly increased by using swept-wavelength interferometer [30], which is an impulse response measurement system using frequency-domain technique. It should be noted that ghost peaks may prevent multiple-point detection based on polarization coupling in PMFs because of second-order mode coupling between polarizations [13], but here the second-order coupling between two LP modes may be negligible because of low power coupling ratio H. If fiber attenuation is neglected, the coupling process of cascaded N coupling points with the same power coupling ratio H can be estimated as

$$
\begin{aligned}
&I_{11}^{(N)} + I_{11}^{(N-1)} + \cdots + I_{11}^{(1)} \\
&= \underbrace{H\left(1-H\right)\cdots\left(1-H\right)}_{N} I_{01} + \underbrace{\left(1-H\right)H\cdots\left(1-H\right)}_{N} I_{01} \\
&\quad + \cdots + \underbrace{\left(1-H\right)\cdots\left(1-H\right)H}_{N} I_{01},
\end{aligned}
\tag{9}
$$

where I_{01} is the launched power of the LP_{01} signal, $I_{11}^{(N)}$ is the received power of the LP_{11} signal generated at the N-th coupling point. Compared to the single-point case, there will be an interference term $(1-H)^{N-1}$ for different LP_{11} signals. For typical low power coupling ratio H less than 0.01 and number of coupling points less than 10, the influence among different coupling points can be neglected. Fig. 5(b) depicts the influence between mode coupling of multiple points. The stress applied at points B and C is 0.3-kgf, while it varies at point A for 0.1, 0.2, and 0.3-kgf. We can see that when the applied stress at point A varies, the fluctuations of the two signals at points B and C are neglected. Fig. 5(c) shows the feasibility of applying different stresses at different points, in which 0.1, 0.2, and 0.3-kgf stresses are applied at points A, B, and C, respectively.

We utilize the experimental setup with Link 3 to investigate the immunity of the proposed scheme to effect of different parameters, as shown in Fig. 3(a). Compared to Link 1, a 3-paddle polarization controller (PC) coiled by the TMF, two fiber rotators attached to a movable and a fixed translation stages, and a thermal cycling chamber (ESPEC, SET-Z-022U-Z) are included in Link 3, which are enabled or disabled to emulate common parameters. All the emulators are initially disabled for each test. The influence of the SOP of probe signal is first studied by enabling the PC and adjusting it arbitrarily for 40 times, and the measurement results are shown in Fig. 6(a). We can see that the power coupling ratio is hardly affected as the polarization changes. Then both fiber rotators are utilized to rotate the TMF for 10 times ranging from 0° to 360° to investigate the influence of stress direction. The power coupling ratio versus stress direction is shown in Fig. 6(b). We can see that the power coupling ratio only varies slightly. The thermal cycling chamber
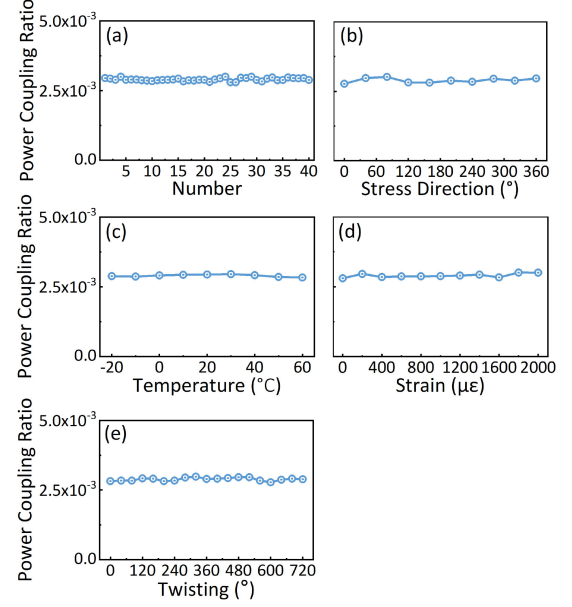

Fig. 6. Power coupling ratio for the measurement of (a) Random polarizations of probe signal for 40 times, (b) Stress direction from 0° to 360°, (c) Temperature from −20-°C to 60-°C, and (d) Strain from 0 to 2000-$\mu\varepsilon$, (e) Twist from 0° to 720°.

scans from −20 to 60-°C to evaluate the temperature response and the power coupling ratio as a function of temperature is shown in Fig. 6(c). We can see that the power coupling ratio only has slight fluctuation over temperature range from −20 to 60-°C. To characterize the strain response, strain is applied within the range from 0 to 2000-$\mu\varepsilon$ by adjusting the movable translation stage, and the power coupling ratio versus the strain are depicted in Fig. 6(d). We can observe that strain has little influence to the power coupling ratio. For the twist response measurement, one of the fiber rotators is utilized to apply twist to the TMF with angles ranging from 0° to 720° and Fig. 6(e) shows the power coupling ratio versus the twist angles. We can see that the variation of the power coupling ratio is slight. So the proposed DTSS is little affected by all these parameters.

IV. CONCLUSION

In this paper, a novel DTSS scheme based on mode coupling in weakly-coupled FMFs is proposed and demonstrated for the first time. Relying on the stress induced coupling behaviors of the LP modes, the dependence of mode coupling to transverse stress is theoretically analyzed and experimentally evaluated. Moreover, the immunity to temperature, strain, twist, stress direction, and SOP are experimentally investigated, which is significant for accurate stress analysis under complex environmental conditions. The scheme can be easily combined with other sensing mechanisms for higher-performance or multiple-parameter measurement.

REFERENCES

[1] A. H. Hartog, *An Introduction to Distributed Optical Fiber Sensors*. Boca Raton, FL, USA: CRC Press, 2017.
[2] I. Matias, S. Ikezawa, and J. Corres, *Fiber Optic Sensors—Current Status and Future Possibilities*. New York, NY, USA: Springer, 2017.

[3] B. Culshaw and J. P. Dakin, *Optical Fiber Sensors: Principles and Components*. Norwood, MA, USA: Artech House, 1988.

[4] X. Bao and L. Chen, "Recent progress in distributed fiber optic sensors," *Sensors*, vol. 12, no. 7, pp. 8601–8639, May 2012.

[5] K. Miah and D. K. Potter, "A review of hybrid fiber-optic distributed simultaneous vibration and temperature sensing technology and its geophysical applications," *Sensors*, vol. 17, no. 11, pp. 2511–2535, Sep. 2017.

[6] P. Lu *et al.*, "Distributed optical fiber sensing: Review and perspective," *Appl. Phys. Rev.*, vol. 6, no. 4, Oct. 2019, Art. no. 041302.

[7] L. Schenato, A. Pasuto, A. Galtarossa, and L. Palmieri, "An optical fiber distributed pressure sensing cable with pa-sensitivity and enhanced spatial resolution," *IEEE Sens. J.*, vol. 20, no. 11, pp. 5900–5908, Feb. 2020.

[8] R. R. J. Maier, W. N. MacPherson, J. S. Barton, S. McCulloch, and B. J. S. Jones, "Distributed sensing using Rayleigh scatter in polarization-maintaining fibres for transverse load sensing," *Meas. Sci. Technol.*, vol. 21, no. 9, Jul. 2010, Art. no. 094019.

[9] T. Feng, J. Zhou, Y. Shang, X. Chen, and X. S. Yao, "Distributed transverse-force sensing along a single-mode fiber using polarization-analyzing OFDR," *Opt. Exp.*, vol. 28, no. 21, pp. 31253–31271, Oct. 2020.

[10] M. Tsubokawa, T. Higashi, and Y. Negishi, "Mode couplings due to external forces distributed along a polarization-maintaining fiber: An evaluation," *Appl. Opt.*, vol. 27, no. 1, pp. 166–173, Jan. 1988.

[11] J. Zhang, V. A. Handerek, I. Çokgör, V. Pantelic, and A. J. Rogers, "Distributed sensing of polarization mode coupling in high birefringence optical fibers using intense arbitrarily polarized coherent light," *J. Lightw. Technol.*, vol. 15, no. 5, pp. 794–802, May 1997.

[12] K. Hotate, K. Makino, Z. He, M. Ishikawa, and Y. Yoshikuni, "High spatial resolution fiber-optic distributed lateral-stress sensing by stepwise frequency modulation of a super structure grating distributed Bragg reflector laser diode," *J. Lightw. Technol.*, vol. 24, no. 7, pp. 2733–2740, Jul. 2006.

[13] D. Song, Z. Wang, X. Chen, H. Zhang, and T. Liu, "Influence of ghost coupling points on distributed polarization crosstalk measurements in high birefringence fiber and its solution," *Appl. Opt.*, vol. 54, no. 8, pp. 1918–1925, Mar. 2015.

[14] X. Chen, H. Zhang, D. Jia, T. Liu, and Y. Zhang, "Implementation of distributed polarization maintaining fiber polarization coupling pressure sensing system," *Chin. J. Laser*, vol. 37, no. 6, pp. 1467–1472, Jul. 2010.

[15] I. Ashry *et al.*, "A review of using few-mode fibers for optical sensing," *IEEE Access*, vol. 8, pp. 179592–179605, Sep. 2020.

[16] L. Jeunhomme and J. P. Pocholle, "Mode coupling in a multimode optical fiber with microbends," *Appl. Opt.*, vol. 14, no. 10, pp. 2400–2405, Oct. 1975.

[17] C. Schulze, R. Brüning, S. Schröter, and M. Duparré, "Mode coupling in few-mode fibers induced by mechanical stress," *J. Lightw. Technol.*, vol. 33, no. 12, pp. 4488–4496, Nov. 2015.

[18] Y. Liu, K. S. Chiang, and P. L. Chu, "Fiber-Bragg-grating force sensor based on a wavelength-switched self-seeded Fabry–Pérot laser diode," *IEEE Photon. Technol. Lett.*, vol. 17, no. 2, pp. 450–452, Feb. 2005.

[19] R. Correia, E. Chehura, S. W. James, and R. P. Tatam, "A pressure sensor based upon the transverse loading of a sub-section of an optical fibre Bragg grating," *Meas. Sci. Technol.*, vol. 18, pp. 3103–3110, Sep. 2007.

[20] F. Ren *et al.*, "Cascaded mode-division-multiplexing and time-division-multiplexing passive optical network based on low mode-crosstalk FMF and mode MUX/DEMUX," *IEEE Photon. J.*, vol. 7, no. 5, Aug. 2015, Art. no. 7902509.

[21] J. Jia *et al.*, "Demonstration of distributed stress sensor based on mode coupling in weakly-coupled FMF," in *Proc. Opt. Fiber Commun. Conf.*, San Diego, CA, USA, 2019, pp. 1–3.

[22] L. Palmieri, "Coupling mechanism in multimode fibers," in *Proc. SPIE*, vol. 9009, Feb. 2014, Art. no. 90090G.

[23] M. K. Barnoski, M. D. Rourke, S. M. Jensen, and R. T. Melville, "Optical time domain reflectometer," *Appl. Opt.*, vol. 16, no. 9, pp. 2375–2379, Mar. 1977.

[24] M. J. Puttock and E. G. Thwaite, "Elastic compression of spheres and cylinders at point and line contact," Nat. Standards Lab., Commonwealth Scientific and Ind. Res. Org., Melbourne, Australia, Tech. Rep. 25, 1969.

[25] L. C. Brezeanu, "Contact stresses between two cylindrical bodies: Cylinder and cylindrical cavity with parallel axes–Part I: Theory and FEA 3D modeling," *Procedia Technol.*, vol. 19, pp. 169–176, Oct. 2015.

[26] H. Kogelnik, "Theory of optical waveguides," in *Guided-Wave Optoelectronics*, T. Tamir, ed. Berlin, Germany: Springer-Verlag, 1990.

[27] D. Marcuse, *Theory of Dielectric Optical Waveguides*. Boston, MA, USA: Academic, 1991.

[28] J. Sakai and T. Kimura, "Polarization behavior in multiply perturbed single-mode fibers," *IEEE J. Quantum. Electron.*, vol. QE-18, no. 1, pp. 59–65, Jan. 1982.

[29] Y. Gao *et al.*, "A degenerate-mode-selective coupler for stable DSP-free MDM transmission," *J. Lightw. Technol.*, vol. 37, no. 17, pp. 4410–4420, Sep. 2019.

[30] N. K. Fontaine, "Characterization of space-division multiplexing fibers using swept-wavelength interferometry," in *Proc. Opt. Fiber Commun. Conf.*, Los Angeles, CA, USA, 2015, pp. 1–3.